8. Kipiniak, Waleriau, "Dynamic Optimization and Control," The M.I.T. Press and Wiley, New York (1961).
9. Lapidus, Leon, et al., *A.I.Ch.E. Journal*, **7**, 288 (1961).
10. Pontryagin, L. S., "The Mathematical Theory of Optimal Processes," Interscience, New York (1962).
11. Rozonoer, L. E., *Automation and Remote Control*, **20** (1959).
12. Thibodeau, R. D., and W. F. Stevens, "Dynamic Optimization," paper accepted for publication in *Chemical and Process Engineering*.
13. ———, Ph.D. thesis, Northwestern University, Evanston, Illinois (1963).

Manuscript received July 17,1963; revision received March 19, 1964; paper accepted March 20, 1964. Paper presented at A.I.Ch.E. Houston meeting.

Fluid-Flow Characteristics of Concurrent Gas-Liquid Flow in Packed Beds

VERN W. WEEKMAN, JR., and JOHN E. MYERS

Purdue University, Lafayette, Indiana

Reactions involving the concurrent flow of liquids and gases through packed beds are becoming increasingly common in both the petroleum and chemical industries. For proper design of these packed reactors, knowledge of the heat transfer and fluid-flow characteristics of the two-phase flow is required. Only one paper (*1*) has been published, dealing with pressure drop and liquid holdup, which covers a fairly wide range of two-phase flow conditions in packed beds. No studies that discuss the problem of heat transfer in packed beds operating with gas-liquid flow have come to the authors' attention.

The present paper deals only with the fluid-flow characteristics; a subsequent paper (*11*) is concerned with the heat transfer studies. An early paper by Piret, Mann, and Wall (*2*) reported a small scattering of pressure-drop data for concurrent gas-liquid flow through packed beds. More

V. W. Weekman, Jr., is with the Socony Mobil Oil Compay, Paulsboro, New Jersey.

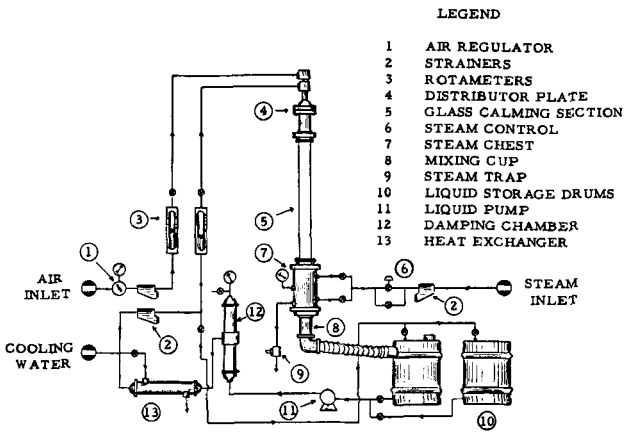

Fig. 1. Flow diagram of experimental apparatus.

recently Larkin (*1*) measured pressure loss and liquid holdup, while Schiesser and Lapidus (3) and Lapidus (*4*) measured liquid and gas holdups by frequency-response techniques. Schiesser and Lapidus also report radial liquid distribution data for trickle-bed conditions with no gas flow. No published data could be found for radial liquid distribution under concurrent gas-liquid conditions.

Pressure-drop data for the air-water system were obtained, as well as pressure-drop data for the foaming type of flow with surfactants present in the liquid phase. Data were also gathered for the velocity, height, distribution, and frequency of liquid pulses observed during the pulsing type of flow.

EXPERIMENTAL EQUIPMENT

A flow diagram of the experimental apparatus is shown in Figure 1. Calibrated rotameters were used to measure the flow of liquid and gas to the top of the packed column. The liquid phase was pumped to a damping chamber consisting of a 2.8 ft. length of 3-in. N.D. (nominal diameter) pipe. Stagnant air maintained in the top section of this chamber served to damp out pump pressure fluctuations and give smooth flow in the rotameters. After it had passed through the column, the liquid was returned to the storage drums.

All thermocouples which supplied data were copper-constantan and were calibrated against a National Bureau of Standards standard thermometer. All pressure gauges were calibrated with a dead weight tester.

A distributor plate, located at the top of the column, consisted of a ¼ in. thick piece of aluminum through which ninety-five evenly spaced, 11/64-in. diam. holes had been drilled.

Three thermocouples were positioned 6¾ in. below the distributor plate at various radii values. These measured the inlet temperature of the two-phase system. Two separate column sections could be positioned between the top support flange and the heat transfer section. One, a 4-ft. glass section, was used for observing flow phenomena. For heat transfer and pressure-drop measurements, a 2-ft. plastic section was installed adjacent to the heat transfer section with a 2-ft. glass visual section installed above. In the flange at the top of the plastic section, thermocouples were located at various radial positions. These thermocouples were used to obtain the bulk inlet temperature.

Pressure taps were drilled into each flange and connected to plastic tubing which ran horizontally to liquid drop-out traps. From the top of each trap, plastic tubing ran to the appropriate manometers. The drop-out traps were drained often, and little liquid accumulation was found. The packing was supported at the bottom of the column by a galvanized wire screen with 7/64-in. by 7/64-in. openings.

An outlet liquid collector was designed and consisted of a thin brass tube positioned in the center of a 3-in. N.D. pipe. This assembly could be flanged to the bottom of the column and allowed the liquid flowing in the outer annular region to be measured. Gas vents assured negligible back pressure owing to the collecting device. Use of two different diameter inner tubes allowed the liquid rate to be measured in two annular sectors, with the center sector liquid rate being obtained by difference.

To determine the structure of the flow at the exit of the bed, an impact tube could be positioned to within ± 0.02 in. across the diameter of the bed. The impact tube was made from ⅛-in. brass tubing with a 0.03-in. wall thickness. This probe was mounted at right angles to the bottom of the bed, and the open end was 1/16 in. below the support screen. A micromanometer was used to measure the impact pressure to the nearest 0.001 in. of water. It was observed that the same profile could be reproduced by traversing from wall to center or from center to wall.

It was noted that when light was passed through the column packed with translucent material, the liquid pulses traversing the column absorbed more light than did the lower density fluid between the liquid pulses. Using a light source on one side of the column and a sensitive photo resistor on the opposite side, one can detect the passage of each pulse and thus measure the pulse frequency. When opaque packing was used, it was possible to reflect light from the rippling surface of the pulse.

The photo resistors employed were of the cadmium sulfide type. A 6-v. storage cell provided the necessary power. The recorder employed was a two-channel d.c. amplifier with low inertia pens capable of resolving signals of 100 cycles/sec. at chart speeds up to 200 mm./sec.

When the pulse velocities were measured, two photo resistors were mounted 1.5 ft. apart, and each was connected to a separate channel on the recorder. The entire glass section was then masked with opaque carbon paper to prevent spurious light from affecting the results. Directly opposite each photo resistor, slits were cut in the masking paper to admit light to the column. A 300-w. source opposite each slit provided the necessary light.

Owing to the sensitivity of the photo cells, each pulse gave a distinctive recorder trace. Thus, by observing the trace of pulses past the first cell, it was possible to identify a given pulse in the trace of the second cell. The time lag between these peaks on the two chart traces enabled the pulse velocity to be measured.

The packing properties are given in Table 1.

FLUID-FLOW MEASUREMENTS

Pressure-Drop Nonfoaming System

While as many as seven regimes of flow have been identified in two-phase flow in pipes (*9*), only three regimes were recognized in the present study for gas-liquid flow through packed beds. A description of these flow regimes follows.

Gas Continuous Flow: The liquid trickles over the packing, and the gas phase flows continuously through the voids in the bed. Visual inspection of the bed indicates that the liquid flows as a laminar film over the packing.

Transition or Rippling Flow: The liquid appears to be in turbulent flow and gives the visual impression of many

Table 1. Packing Properties

Type	Average diameter, in.	Packing void fraction	Thermal (*5, 6, 7*) conductivity, B.t.u./(hr.)(ft.)(°F.)
TCC beads	0.149	0.378	0.21
Glass spheres	0.187	0.390	0.3-0.44
Alumina spheres	0.255	0.430	0.13-0.10

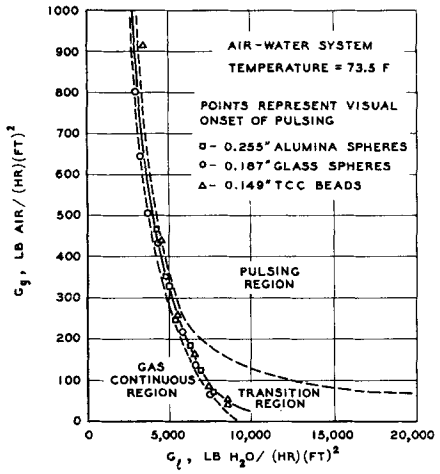

Fig. 2. Flow regimes for concurrent air-water flow.

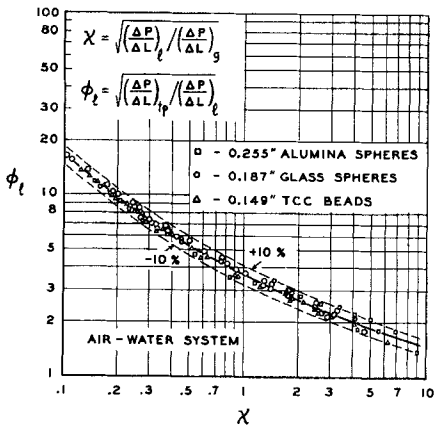

Fig. 3. Correlation of concurrent two phase pressure drop in packed beds.

small ripples. During this rippling type of flow, occasional pulses may be observed near the bottom of the column.

Pulsing Flow: The pulses first observed in transition flow are now readily apparent and traverse the entire column. These pulses appear to be composed of liquid and present a sharp leading edge, while the trailing edge of the pulse tapers off in the form of a wake. Larkin et al. (*1*) also observed these pulses in a 4-in. column and described them as "'flat plugs of high density material flowing down the column."

Figure 2 shows where these flow regimes occur in relation to the gas and liquid rates. The points on the curve represent the first visual observation of pulses, while the dotted lines enclose the visually observed transition or rippling flow region. Thus, at low liquid rates it is possible to attain very high gas rates and still remain in the gas-continuous region; at high liquid rates, even very low gas rates give the transition or rippling flow regime. The pulsing mode was observed up to the limits of the flow rates studied.

The transition from one flow regime to another appeared to have no effect on the pressure drop through the bed. It was observed, however, that pulsations in the manometers were greatest at the transition from gas continuous to the pulsing regime of flow. When pulsations were encountered, an arithmetic average reading was used. No significant differences in pressure drop per foot of bed were observed for the various column sections.

One of the more useful correlations of two-phase flow in pipes is given by Lockhart and Martinelli (*10*). The first extension of this work to packed beds came to the authors' attention in an unpublished report (*5*). Lockhart and Martinelli derive four simple dimensionless variables, using the Blasius form of the friction factor, which correlate two-phase flow data in pipes for a wide range of systems and conditions. As shown below, their analysis may be extended to include two-phase flow in packed beds. The analysis rest on two plausible postulates.

1. In two-phase flow the static ΔP for the liquid phase is the same as for the gas phase, regardless of the flow mechanism.
2. The liquid volume plus the gas volume equals the void volume in the packed bed.

If one considers a packed bed to consist of λ channels of equivalent diameter D_c and total bed length L, then

$$\text{Void volume} = \epsilon L \pi D_t^2/4 = \lambda L \pi D_c^2/4 \qquad (1)$$

It is possible to define hydraulic diameters D_l and D_g for the liquid and gas, respectively, when the bed is operating under two-phase flow conditions. One can further define two factors α and β such that

$$\alpha = \frac{A_l}{\pi D_t^2/4} \qquad \beta = \frac{A_g}{\pi D_g^2/4} \qquad (2)$$

where A_l and A_g are the actual flow areas of the liquid and gas, respectively, at any cross section under two-phase flow conditions.

The variables D_l and D_g as well as α and β may be functions of the liquid and gas flow rates as well as of the packing characteristics. Of course, λ and D_c will be functions of the packing used.

Based on postulate (2) the flow areas must add up to the total area. Thus

$$\alpha \pi D_t^2/4 + \beta \pi D_g^2/4 = \lambda \pi D_c^2/4 \qquad (3)$$

The liquid and gas saturations are then readily defined as

$$R_l = \frac{\alpha D_t^2}{\lambda D_c^2} \qquad R_g = \frac{\beta D_g^2}{\lambda D_c^2} \qquad (4)$$

When one follows Lockhart and Martinelli's derivation (*10*), it is possible to derive the function ϕ_l as applied to packed beds (*8*):

$$\phi_l^2 = \left(\frac{\Delta P}{\Delta L}\right)_{tp} \Big/ \left(\frac{\Delta P}{\Delta L}\right)_l = \left(\frac{\alpha}{\lambda}\right)^{n-2} \left(\frac{D_l}{D_c}\right)^{n-5}$$

For the gas a similar function ϕ_g can be shown to be

$$\phi_g^2 = \left(\frac{\Delta P}{\Delta L}\right)_{tp} \Big/ \left(\frac{\Delta P}{\Delta L}\right)_g = \left(\frac{\beta}{\lambda}\right)^{m-2} \left(\frac{D_g}{D_c}\right)^{m-5}$$

where m and n are the Blausius friction factor plot slopes for gas and liquid, respectively.

Thus it is possible to express the essentially unmeasurable dimensionless variables α/λ, β/λ, D_l/D_c, D_g/D_c with the measurable dimensionless variables of ϕ_l, ϕ_g, R_l, and R_g.

The functions ϕ_l or ϕ_g do not contain all the variables which affect two-phase flow. Using postulate (1) and observing that $n = m$ from single-phase flow data, one can derive another function χ (*8*):

$$\chi^2 = \left(\frac{\Delta P}{\Delta L}\right)_l \Big/ \left(\frac{\Delta P}{\Delta L}\right)_g = \frac{\phi_g^2}{\phi_l^2}$$

The function χ^2 contains the variables not accounted for by ϕ_g^2 and ϕ_l^2 (*8*). Thus, one might hopefully expect χ^2 to be a function of ϕ_l^2 and ϕ_g^2.

Figure 3 presents a correlation of the present pulsing and transition flow data based on the ϕ_l and χ factors.

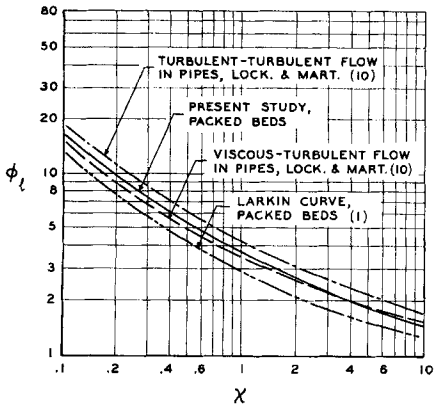

Fig. 4. Comparison of pressure drop correlation with previously published correlations.

The ϕ_l and χ factors were plotted instead of ϕ_l^2 and χ^2 to reduce the log cycles required. From Figure 3 it can be seen that all data fell within ± 10% of best line through the data.

The data represent water rates from 1,250 to 25,000 lb./(hr.)(sq. ft.) and air rates from 50 to 1,200 lb./(hr.)(sq. ft.) for three packing sizes for which D_t/D_p ranged from 11.8 to 20. The data for the gas-continuous region did not correlate with the other two regions of flow and fell considerably below the correlation of Figure 3.

Figure 4 compares the current two-phase correlation with that obtained by Larkin et al. for packed beds and Lockhart and Martinelli for pipes. It can be seen that the present correlation falls between the turbulent liquid-turbulent gas and the viscous liquid-turbulent gas curves of Lockhart and Martinelli. This is indeed remarkable when one considers that their data represent two-phase flow through horizontal pipes. Thus, a large number of channels in the packed bed may function in the same fashion as pipes in two-phase, concurrent flow.

The Larkin et al. curve is significantly lower than the other curves because they chose to correct their experimental pressure drop results for the mean density in the vertical column. This mean density was defined as

$$\rho_m = R_l \rho_l + (1 - R_l)\, \rho_g$$

Since their measured values of R_l vary for most of the data from 0.1 to 0.5, the quantity ρ_m varies from about 6.0 to 31 lb./(cu. ft.) for the two-phase flowing mixture. This definition of the mean density is based on the total volume of liquid held up in the bed and neglects the fact that a significant amount of the liquid is supported by the packing and does not contribute to the static pressure gradient in the column. It is a common observation that substantial amounts of liquid will be held in a packed bed under static conditions for which the static pressure gradient will be zero. Thus, the static pressure drop in the flowing column will be less than the drop calculated with ρ_m used as the flowing density. It is also possible to compare the average velocity predicted from this value of ρ_m with that actually measured during pulsing flow. From Table 2, it can be seen that the experimentally determined pulse velocity is as much as four times that predicted with the Larkin et al. definition of ρ_m. Appropriate values of R_l were obtained from Larkin et al.'s correlation (*1*). As will be shown later, the average velocity in the bed is even higher than the pulse velocity. It is thus probable that the static pressure gradient is negligible compared with the pressure drop for liquid loadings less than 25,000 lb./(hr.)(sq. ft.). Of course, as the liquid loading approaches the point where the bed is filled with liquid, a static pressure correction would have to be applied. The remarkably close agreement of the present packed bed correlation to the Martinelli and Lockhart correlation for pipes is also significant, since all their data were taken in horizontal pipes for which no correction for mean density was necessary.

Pulse Measurements—Nonfoaming System

When the liquid or gas rate was adjusted to cause the flow regime to change from gas continuous to pulsing flow, a rippling or transition-flow regime was always observed. At high gas rates this flow regime would change readily to pulsing flow with only slight gas or liquid rate increases. At liquid rates greater than 10,000 lb. water/(hr.)(sq. ft.), no distinguishable gas-continuous region was noted, even at the lowest gas rates employed [that is 25 lb. air/(hr.)(sq. ft.)].

As the flow regime changes from gas-continuous flow to pulsing flow, it is possible to describe in a qualitative fashion the changes occurring in the bed. Assume that the liquid rate is 5,000 lb. water/(hr.)(sq. ft.), and the gas rate is increased from zero to 500 lb. air/(hr.)(sq. ft.). As seen in Figure 2, the pulsing region begins at about 325 lb./(hr.)(sq. ft.). The gas-continuous region of flow likely includes laminar-liquid, laminar-gas flow as well as laminar-liquid, turbulent-gas flow. As the gas rate is increased, it will cause a greater velocity in the liquid phase by increasing the drag force on the liquid phase. As this rate is further increased, the drag force can become sufficient to cause turbulence in the liquid phase, particularly at channel constrictions. Also some liquid may become separated from the liquid film and move as slugs or drops down a channel before reforming over the packing. This type of flow is typical of the rippling or transition region, and the turbulence of the liquid phase can be visually observed through the glass wall. As the gas rate is again increased, the separated slugs or drops are now large enough to bridge channels. This momentary blocking of some channels causes increased flow in others and thus increases the chance of separation and blocking in parallel channels. This disturbance would thus tend to propagate down the bed as pulses or waves.

Initially, the pulses are always seen to begin in the lower part of the bed, while rippling flow is occurring in the top part. Since slightly larger velocities will exist at the bottom owing to the lower pressure of the gas phase at this point, the separation of liquid drops or slugs would first occur in this region. With slightly higher gas and liquid rates, the pulses begin within 6 in. of the top and traverse the entire column.

It was observed that at the higher liquid rates, there was a tendency for the pulses to coalesce as they moved down the column. Thus, the frequency of the pulses would be slightly lower at the bottom than at the top. For liquid rates up to 10,000 lb. water/(hr.)(sq. ft.) there was,

TABLE 2. EFFECT OF MEAN DENSITY ON VELOCITY

0.187-in. diameter glass beads, $\epsilon = 0.39$

$\rho_m = R_l \rho_l + (1 - R_l)\, \rho_g$ (*1*)

$V_m = \dfrac{G_l + G_g}{\rho_m \epsilon}$ $\quad V_p$ = Experimental pulse velocity

G_l, lb. water (hr.)(sq. ft.)	G_g, lb. air (hr.)(sq. ft.)	ρ_m, lb. cu. ft.	V_m, ft. sec.	V_p, ft. sec.
5,000	600	7.03	0.57	1.65
7,500	600	8.31	0.69	3.00
10,000	650	10.76	0.69	3.04
15,000	450	12.96	0.95	3.41

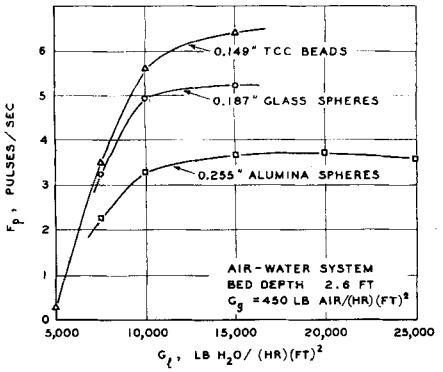

Fig. 5. Effect of packing size on pulsing frequency.

however, no appreciable frequency change down the column.

Figure 5 presents the effect of liquid rate and particle diameter on pulse frequency. Thus, decreasing the particle size increases the pulsing frequency, while increasing the liquid rate up to approximately 15,000 lb. water/(hr.)(sq. ft.) also increases the pulse frequency. At higher liquid rates the frequency actually declines owing to increasing coalescence of the pulses. Increasing air rate always gives increasing pulse frequency. Figure 6 shows the effect of air and water rates on the velocity of the pulses. In general, the pulse velocity increases with increases of either gas or liquid rate.

A pulsing unit is defined as the distance from the leading edge of a pulse to the leading edge of the following pulse. Thus, a pulsing unit contains an entire liquid pulse and the lower density region behind it. The height of such a pulsing unit may be obtained by dividing the pulse velocity by the the pulse frequency:

$$H_t = V_p/F_p$$

Figure 7 presents the effect of liquid rate on H_t for various constant gas rates. For all rates studied, it can be seen that H_t exhibits a pronounced minimum at approximately 10,000 lb. water/(hr.) (sq. ft.). At water rates less than this, H_t rapidly increases as the water rate decreases. This result seems reasonable, since the pulse velocity will not exceed the air velocity, and the frequency of liquid pulses will tend toward zero as the water rate approaches zero. One value of H_t was measured at 13.4 ft. at G_l = 3,000 lb. water/(hr.) (sq. ft.) and G_g = 800 lb. air/(hr.) (sq. ft.). The increase in H_t as the liquid rate is increased beyond 10,000 lb. water/(hr.) (sq. ft.) is due to F_p decreasing while V_p is increasing. This decrease in F_p is due to the liquid portion of the pulse becoming longer from coalesence. The same liquid volume could be carried by shorter pulses of higher frequency, but this

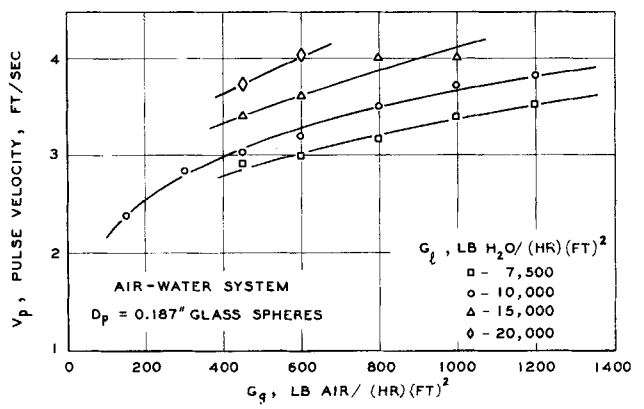

Fig. 6. Effect of gas rate on pulse velocity.

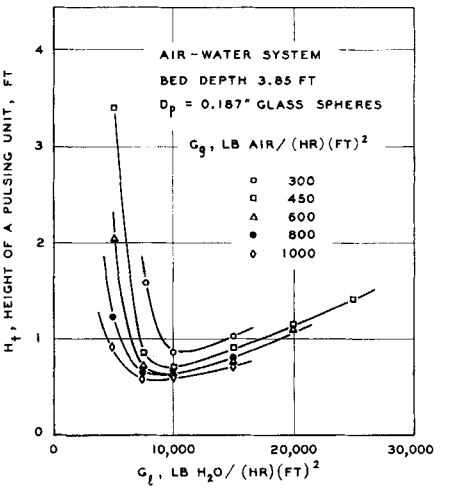

Fig. 7. Effect of liquid rate on height of a pulsing unit.

would represent a higher energy loss because of the greater amounts of liquid surface generated. Thus, the flow regime attains the more stable configuration of longer pulses. Figure 7 also shows that H_t decreases with increasing gas rate for all data obtained.

To measure the height h_t of the liquid, or more dense portion of the pulse, high-speed still pictures and motion pictures were taken of the bed during pulsing flow. It proved difficult to obtain accurate heights for the pulses because, although the leading edges were sharp and distinct, the trailing edges had no distinct endings. Thirty parts per million of the blue dye Xylene Cyanole FF helped to enhance the visibility of the pulses during the photographic work. Table 3 contains the heights of the liquid pulses h_t as obtained from the high-speed photography. Shown for comparison are the calculated heights for the whole pulsing unit H_t. In general, h_t decreased as the gas rate was increased at constant liquid rate.

It was noted that changing the centrifugal pump speed, and even removal of the distributor plate, gave no measurable change in either pulse frequency or velocity.

Liquid Distribution Measurements

Typical data obtained from the exit liquid collector assembly have been plotted on Figure 8 as the mass rate of liquid flow through each of the three radial sectors. The data for zero air rate generally agree with those of Schiesser and Lapidus (3) in that the flow tends to concentrate near the wall and also at the center of the bed. The effect of increasing air rate is generally to decrease the liquid

TABLE 3. HEIGHT OF LIQUID PULSES BY PHOTOGRAPHY

D_p = 0.187-in. Glass spheres, concurrent air-water flow

G_l, lb. water/(hr.)(sq. ft.)	G_g, lb. air/(hr.)(sq. ft.)	h_t, in.	H_t, in. (from figure 7)
3,000	1,000	0.5	61.5
5,000	450	2	41.0
5,000	600	1.5	24.5
5,000	1,000	0.75	11.0
7,500	450	2	10.1
7,500	1,000	0.75	7.1
10,000	300	3	10.1
10,000	800	2	7.9
10,000	1,000	1.5	7.4
15,000	300	3	12.2
15,000	800	3	9.8
20,000	300	4	12.6
25,000	300	9	35.0

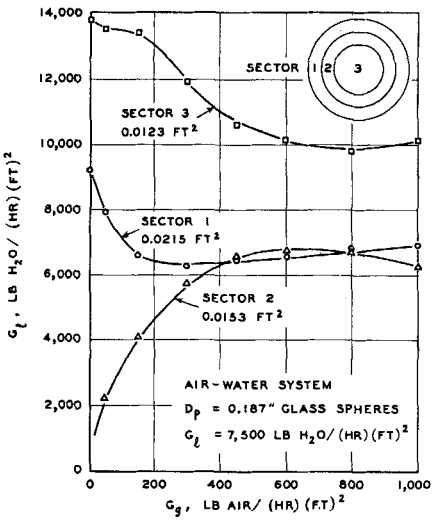

Fig. 8. Outlet liquid distribution.

mass velocity at the center as well as at the wall. It can be seen that for pulsing flow, the mass velocity is highest at the center of the bed with a fairly uniform distribution in the rest of the bed. Thus, increasing the air rate has the general effect of giving a more uniform radial liquid distribution.

Impact Tube Measurement

An impact tube traverse revealed further information on the structure of the flow at the exit of the packed bed. The pressure increase due to the impact of a moving fluid is given by $\Delta P = V^2 \rho/2g_c$. Since air and water differ in density by a factor of approximately 300, the dominant variable in the above equation will be the density. The impact pressure measurement is complicated by the presence of entrained water in the gas phase, which would give considerably lower impact pressures than a continuous water phase. Even at the highest liquid rate employed, the mean density of an air-water system, calculated from the volume fraction of flowing liquid, would be about one/fortieth the density of water. It thus appears that the greatest impact pressure would be imparted by the liquid-continuous portions of the flow.

Figure 9 shows the results of impact tube traverses at 15,000 lb. water/(hr.) (sq. ft.) for various gas rates. The highest impact pressures were observed nearest the wall and decreased rapidly to a point 0.8 in. from the wall; the profile thereafter remained essentially constant. The impact profile was considerably lower near the wall when the gas rate was less than that required to sustain pulsing flow. With gas flow only, the profile was essentially flat.

Although two-phase flow precludes any absolute velocity calculations, it is apparent from Figure 9 that the distribution of consolidated liquid across the radius is not uniform and that the more dense liquid flow occurs near the walls. This result bears out the visual observation that the pulses contain a high concentration of liquid. Since the distribution measurements showed that the liquid rate was highest at the center, while the impact pressure was lowest at this point, the implication is that most of this liquid must be flowing as entrained drops or spray in the center region.

Proposed Model for Pulsing Flow

The simplest model for pulsing flow, which would agree with the visual observations, would require the liquid pulses to bridge the entire bed. For this model all the gas would be in the gas portion of the pulse unit and all the liquid in the liquid portion. With this model the liquid and gas would have the same velocity. The total volume per hour of both gas and liquid is given as follows:

$$\text{Total vol./hr.} = \frac{W_l}{\rho_l} + \frac{W_g}{\rho_g}$$

Dividing this rate by ϵA (the total available cross-section area) one gets the desired velocity:

$$V_{NS} = \frac{1}{\epsilon}\left[\frac{G_l}{\rho_l} + \frac{G_g}{\rho_g}\right]$$

V_{NS} represents the velocity of the pulses if both liquid and gas travel at same velocity (that is no slip velocity between phases). Calculated values of V_{NS} were from one and one-half to two and one-half times as great as the experimentally measured pulse velocity (V_p).

It is apparent, then, that the nonslip model does not fit the experimental facts. If, however, it is assumed that the liquid pulses do not extend across the entire column diameter, a more reasonable model may be postulated. The liquid distribution data show that the liquid rate is greater in the center of the column, and the impact data imply that this liquid is not consolidated but rather entrained by the air stream. Since the impact data, as well as visual observations, show that the more consolidated liquid flow appears near the walls, a reasonable model for the pulses would be that of a wavelike torus. The pulses are represented as similar to waves which completely encircle the walls and have a sharp leading edge and a trailing wake. The impact traverse measurements would indicate that the pulses extend into the bed approximately 4 to 5 particle diameters for the 0.187-in. diameter glass spheres. If it is assumed that all the liquid trapped in sector 1 of the liquid collector is contained in the pulses, then potentially 30 to 35% of the total liquid may be traversing the bed as pulses.

Pressure Drop—Foaming System

The presence of a surfactant in the liquid phase has a significant effect on the flow regime and pressure drop for two-phase flow through a packed bed. At low gas and liquid rates, the pressure drops with surfactants present were identical with air-water flow; however, as the rates increased, the flow regime abruptly changed to the foaming type of flow and the pressure drop increased from five to fortyfold, depending on the surfactant used. Figure 10 shows a typical effect of surfactant concentration on the two-phase pressure drop. The initial maximum-minimum in the pressure drop curve for the higher surface concentration was observed for all three packing sizes and all liquid rates. To explain this most interesting phenomenon, it is necessary to consider the dynamic surface tension effect, since at an agitated liquid-gas interface it will be higher than the static value of the surface tension.

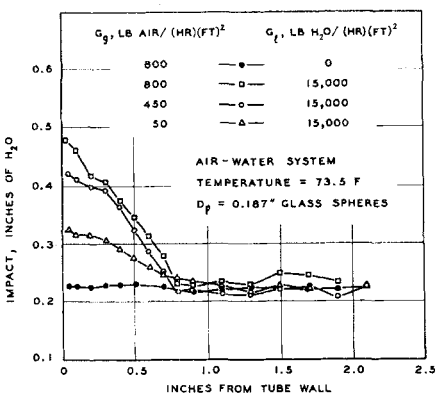

Fig. 9. Effect of gas rate on impact profile.

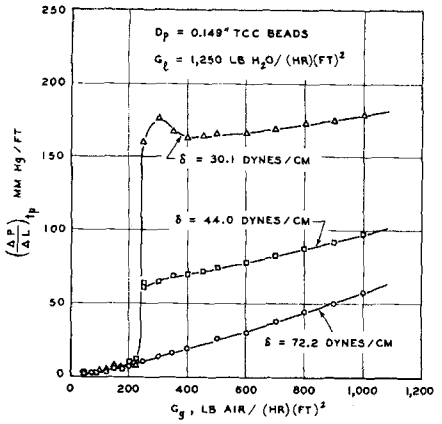

Fig. 10. Effect of surfactant OT-75 on pressure loss.

The minimum in the pressure drop curve (shown on Figure 10) may now be explained as the resultant of two opposite effects, an increasing pressure drop due to increasing gas rate and a decreasing pressure drop due to increasing dynamic surface tension. With increasing dynamic surface tension, the stability of the foam bridging the packing channels decreases, thus tending to lower the pressure drop. Thus, the increasing gas rate increases the pressure drop as expected; however, the increasing air rate also gives an increasing dynamic surface tension which, as explained above, will result in a lower pressure drop. The net result of these two opposite effects is to give a minimum in the pressure drop curve as the gas rate is increased in the foaming region.

It was found that the transition to foaming flow occurred at much lower flow rates than the transition to pulsing flow with pure water. This could be explained by the fact that the higher surface tension of pure water will not allow as thin a film to bridge a channel. Different surfactants gave different transition points (*8*).

The foaming data would not fit the ϕ_g vs. χ type correlation. Larkin et al. (*1*), who used a foaming soap solution, also found considerable scatter from the ϕ_g vs. χ type correlation. The χ parameter was modified as follows:

$$\chi' = \left(\frac{\Delta P}{\Delta L}\right)_l^{0.5} \Big/ \left(\frac{\Delta P}{\Delta L}\right)_g$$

With the χ' basis, a single curve correlated the data for a given surfactant concentration (*8*).

SUMMARY

Liquid pulses are observed as a naturally occurring phenomenon for two-phase gas-liquid flow in packed beds. It was determined that these pulses do not bridge the entire column diameter but rather have the shape of a wavelike torus. The thickness of the pulses exhibit a minimum with increasing liquid rates due to a coalesence phenomena.

Similar relations correlate the pressure drop results for two-phase flow in both pipes and packed beds. No sharp transition in pressure drop was observed at flow regime transition points for the air-water system. Surfactants have a profound effect on flow regime transition and pressure drop in the air-water system.

ACKNOWLEDGMENT

The financial aid of the Socony Mobil Oil Co., through the Employee Incentive Fellowship awarded to V. W. Weekman, Jr., is gratefully acknowledged.

NOTATION

A_o = cross-sectional area of empty tube, sq. ft.
A_g = cross-sectional area for gas flow, sq. ft.
A_l = cross-sectional area for liquid flow, sq. ft.
D = diameter, ft.
f = fanning friction factor
F_p = pulse frequency, pulses/sec.
G = mass velocity based on empty tube area, lb./(hr.)(sq. ft.)
g_c = dimensional constant
h = height of liquid or gas section of pulse, ft.
H_t = total height of a pulsing unit, ft.
L = linear dimension, ft.
m = slope of Blasius type of friction factor plot for liquid
n = slope of Blasius type of friction factor plot for gas
R = fraction of void volume occupied by gas or liquid
V_p = pulse velocity, ft./sec.
V_{NS} = velocity of two phase flow when no slip exists between phases, ft./sec.
W = mass rate, lb./(hr.)

Greek Letters

α,β = dimensionless constants
$\Delta P/\Delta L$ = pressure drop per foot of bed, mm. Hg/ft.
ϵ = fraction void space in packed bed
λ = number of equivalent channels in packed bed
$\chi^2 = \left(\frac{\Delta P}{\Delta L}\right)_l \Big/ \left(\frac{\Delta P}{\Delta L}\right)_g$
$\chi' = \left(\frac{\Delta P}{\Delta L}\right)_l^{0.5} \Big/ \left(\frac{\Delta P}{\Delta L}\right)_g$
$\phi_g^2 = \left(\frac{\Delta P}{\Delta L}\right)_{tp} \Big/ \left(\frac{\Delta P}{\Delta L}\right)_g$
$\phi_l^2 = \left(\frac{\Delta P}{\Delta L}\right)_{tp} \Big/ \left(\frac{\Delta P}{\Delta L}\right)_l$
μ = viscosity, lb./(hr.)(ft.)
ρ = density, lb./cu. ft.

Subscripts

c = channel
g = gas
l = liquid
m = mean
NS = nonslip
p = pulse
tp = two phase
t = tube

LITERATURE CITED

1. Larkin, R. P., R. R. White, and D. W. Jeffrey, *A.I.Ch.E. Journal*, **7**, No. 2, p. 231 (1961).
2. Piret, E. L., C. A. Mann, and T. Wall, Jr., *Ind. Eng. Chem.*, **32**, 861 (1940).
3. Schiesser, W. E., and Leon Lapidus, *A.I.Ch.E. Journal*, **7**, 163 (1961).
4. Lapidus, Leon, *Ind. Eng. Chem.*, **49**, 1,000 (1957).
5. Private communication from H. Grayson, Engineering Dept., Socony Mobil Oil Company, New York.
6. McAdams, W. H., "Heat Transmission," 3 ed., McGraw-Hill, New York (1954).
7. Mischke, R. A., and J. M. Smith, *Ind. Eng. Chem. Fundamentals*, **1**, 288 (1962).
8. Weekman, V. W., Jr., Ph.D. thesis, Purdue University, Lafayette, Indiana (1963).
9. Baker, O., *Oil Gas Journal*, **54**, No. 11, 185 (1954).
10. Lockhart, R. W., and R. C. Martinelli, *Chem. Eng. Progr.*, **45**, 39 (1949).
11. Weekman, V. W., Jr., and J. E. Meyers, *A.I.Ch.E. Journal*, to be published.

Manuscript received July 3, 1963; revision received March 13, 1964. Paper accepted March 13, 1964. Paper presented at A.I.Ch.E. Houston meeting, December, 1963.